J. Meas. Sci. Instrum., 2025, 16(2): 186-194. http://jmsi.publish.founderss.cn
DOI: 10.62756/jmsi.1674-8042.2025018 jmsi@nuc.edu.cn

A centroid measurement method based on 3D scanning

HE Xin[1], LI Zhen[2*]

1. Engineering Training Center, Tianjin University of Technology and Education, Tianjin 300222, China;
2. School of Mechanical Engineer, Tianjin University of Technology and Education, Tianjin 300222, China

***Corresponding author:** LI Zhen (kernelHX@126.com)

Received: November 4, 2024 **Revised:** December 23, 2024 **Accepted:** February 23, 2025

Abstract: The centroid coordinate serves as a critical control parameter in motion systems, including aircraft, missiles, rockets, and drones, directly influencing their motion dynamics and control performance. Traditional methods for centroid measurement often necessitate custom equipment and specialized positioning devices, leading to high costs and limited accuracy. Here, we present a centroid measurement method that integrates 3D scanning technology, enabling accurate measurement of centroid across various types of objects without the need for specialized positioning fixtures. A theoretical framework for centroid measurement was established, which combined the principle of the multi-point weighing method with 3D scanning technology. The measurement accuracy was evaluated using a designed standard component. Experimental results demonstrate that the discrepancies between the theoretical and the measured centroid of a standard component with various materials and complex shapes in the X, Y, and Z directions are 0.003 mm, 0.009 mm, and 0.105 mm, respectively, yielding a spatial deviation of 0.106 mm. Qualitative verification was conducted through experimental validation of three distinct types. They confirmed the reliability of the proposed method, which allowed for accurate centroid measurements of various products without requiring positioning fixtures. This advancement significantly broadened the applicability and scope of centroid measurement devices, offering new theoretical insights and methodologies for the measurement of complex parts and systems.

Key words: centroid measurement; mass characteristic parameter; 3D scanning; 3D point cloud data; no specialized positioning fixtures; multi-point weighing method

0 Introduction

Mass characteristic parameters are fundamental indicators that define the mechanical properties of an object, mainly encompassing mass, centroid, moment of inertia, and product of inertia[1-3]. They are critical for theoretical calculations and practical applications in dynamic configuration, posture control, and precise trajectory management of moving objects[4-6]. For instance, precision control of the centroid is essential in products such as aircraft, ships, ejection seats, and missiles, necessitating accurate measurement of their centroid coordinates[7,8]. Consequently, developing specialized measurement equipment for mass characteristic parameters is imperative during product development.

The multi-point weighing method is one of the most widely used and mature techniques in the field of centroid measurement[9-11]. This method is based on the principle of static moment balance, where the centroid coordinate is determined across various states. This method requires a strict geometric constraint relationship between the object being measured and the sensor support point, which leads to inherent defects. First, the measurement platform needs to be customized with special positioning fixtures according to the size of the test piece[12,13]. Second, for asymmetric special-shaped parts, the reference plane conversion error during multiple posture adjustments will form error accumulation[14,15]. Third, the structural deformation caused by contact measurement may cause the center of mass coordinate deviation. These limitations seriously restrict the accuracy of traditional methods of center-of-mass measurement[16].

Researchers have carried out a series of improvements to solve the problems. Zhao et al.[17] proposed a set of combined measurement systems for centroid measurement of large-sized rotating parts. The distance can be adjusted according to the length of the part and the supporting position to adapt to different lengths. Wang et al.[18] designed a novel structure to adjust the mobile

platform to eliminate side forces that might load on the load cells. It was proved that the repeatability of the proposed structure was higher than the traditional one and there were no side forces by simulations. Gonzalo et al.[19] proposed a fast 3D measurement method of the centroid in a tiltrotor-type aircraft using photogrammetry and scales without previous leveling of the aircraft. This greatly improves the versatility of the centroid measurement method. However, existing improvement solutions all require customized test equipment and positioning fixtures[20]. Any difference between the actual state of the test object and the theoretical state will directly affect the measurement results.

To tackle these challenges, we present a universal centroid measurement method based on 3D scanning, facilitating high-precision measurements across a diverse array of product types and geometries. The method can be completed on the same platform for parts of different product shapes, materials, and qualities, without the need for custom fittings, greatly improving the versatility of the platform, reducing the test cost, and providing technical support for the future to adapt to the centroid measurement of multiple models and different types of products.

1 Materials and methods

1.1 Configuration of centroid measurement system

As shown in Fig.1, the centroid measurement system features a specimen stage equipped with four support components, which is fixed on the optical platform. Each support component consists of a Z-axis linear translation stage, a weighing sensor, and a support ball from bottom to top, whose positions can be adjusted as needed. The weighing sensor is a high-precision column mass sensor with a measuring range of 50 kg, a relative error of less than $\pm 0.3\%$, and a safe overload range of 150% of full scale. The stage is placed on top of the support components, ensuring that the upper and lower surfaces remain parallel and flat. Before measurement, scanning markers are applied to both the test object and the stage. During measurement, the object is placed on the stage in any stable orientation, and the weight variations are recorded by each weighing sensor. Subsequently, a scanner is employed to capture 3D data of the test object, the specimen stage, and the support balls. The Creaform HandySCAN 700 scanner is used to obtain point cloud data with a resolution of 0.05 mm, an accuracy of 0.03 mm, a volume accuracy of 0.02 mm+0.06 mm/m, and a scan area of 275 mm×250 mm.

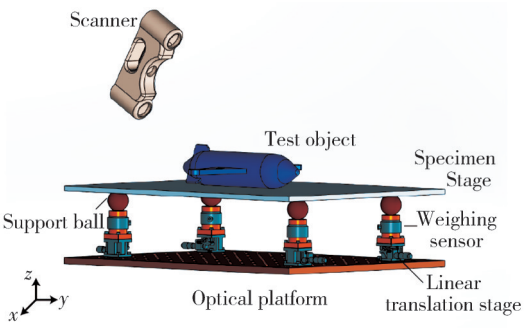

Fig. 1 Overall design of centroid measurement system based on 3D scanning

1.2 Centroid measurement model based on 3D scanning

Traditional centroid measurement methods often require customized devices and precise fixtures, leading to elevated development costs and low equipment utilization. The centroid measurement method is based on 3D scanning technology, effectively addressing its limitations. This integration significantly expands the application range of the method and enhances measurement accuracy. Before measurement, it is necessary to use the Z-axis height adjuster to adjust the stage to a horizontal level. In one of the measurements, the 3D point cloud data of the test object, the specimen stage, and the support balls captured by the scanner are processed to calculate the centroid of the object, as illustrated in Fig.2.

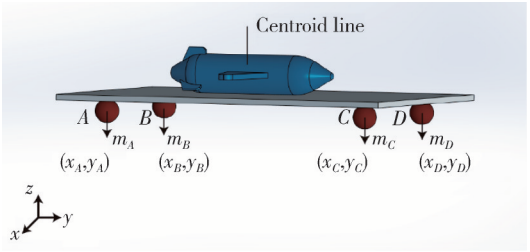

Fig. 2 Schematic diagram of centroid line

The coordinate system is aligned with the plane of the specimen stage, establishing the Z axis and laying out the plane of the specimen stage. The support balls are fitted to determine the coordinates of their centers. Using the mass measurements from the sensors of each support component, the projection of the centroid onto the XY plane can then be calculated by

$$\begin{cases} x = \dfrac{x_A m_A + x_B m_B + x_C m_C + x_D m_D}{m_A + m_B + m_C + m_D}, \\ y = \dfrac{y_A m_A + y_B m_B + y_C m_C + y_D m_D}{m_A + m_B + m_C + m_D}, \end{cases} \tag{1}$$

where x_i, y_i, m_i $(i=A,B,C,D)$ represent the X-axis and Y-axis coordinates of the centroid of the support balls and the measured mass from the weighing sensors of each

support component. Once the projected coordinates of the centroid in the XY plane are obtained, a line parallel to the Z axis can be drawn through this point, resulting in the centroid line l_i for the measured state.

In another measurement, the orientation of the test object on the specimen stage was altered to obtain the centroid line for this new state. For objects that cannot be easily positioned in different orientations for measurement, auxiliary supports can be employed. These auxiliary supports are affixed to the specimen stage, and before loading the measured object, the weighing sensors are zeroed out to ensure accurate measurements, as illustrated in Fig.3. The auxiliary supports serve solely to adjust the object's orientation during testing and does not impose specific requirements on the object itself. Thus, this method provides significant convenience for measuring objects that lack reliable supporting surfaces.

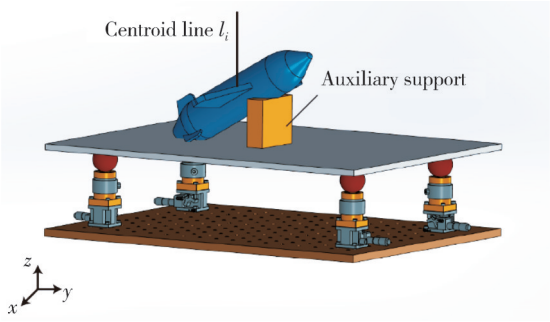

Fig. 3 Auxiliary support for orientation change of test object

After obtaining two or more centroid lines of the test object, the centroid lines are transformed into the same coordinate system based on the object point cloud data. Taking the theoretical model of the object as the standard, the point cloud and centroid line of the object in each measurement are converted to the coordinate system of the theoretical model. The transformation matrix for the ith point cloud of the object can be denoted as $\boldsymbol{T}_i$. The centroid line for the ith measurement L_i, once transformed into the theoretical model coordinate system, can be calculated by

$$L_i = l_i \boldsymbol{T}_i. \tag{2}$$

$(\vec{I},\vec{J},\vec{K})$ are the three coordinate axes of the theoretical model's coordinate system, and $(\vec{i},\vec{j},\vec{k})$ are the three coordinate axes of the global coordinate system (the specimen stage coordinate system). In the initial state, $(\vec{I},\vec{J},\vec{K})$ is the same as $(\vec{i},\vec{j},\vec{k})$. When the test object is rotated, the two coordinate systems are inconsistent, and there is

$$(\vec{i},\vec{j},\vec{k}) = (\vec{I},\vec{J},\vec{K})\boldsymbol{R}, \tag{3}$$

where $\boldsymbol{R}$ represents the transition matrix between the two coordinate systems. $\boldsymbol{R}$ is the 3rd order rotation matrix, which can be expressed as

$$\boldsymbol{R} = \boldsymbol{e}\boldsymbol{e}^{\mathrm{T}} + (\cos\varphi)(\boldsymbol{I} - \boldsymbol{e}\boldsymbol{e}^{\mathrm{T}}) + (\sin\varphi)\boldsymbol{E}, \tag{4}$$

where $\boldsymbol{e} = [e_1,\ e_2,\ e_3]^{\mathrm{T}}$ represents the direction of the rotation axis; φ represents the angle of rotation of the stage coordinate system relative to the model coordinate system; $\boldsymbol{I}$ is the unit matrix; and $\boldsymbol{E}$ is the cross-product matrix of $\boldsymbol{e}$, that is

$$\boldsymbol{E} = \begin{bmatrix} 0 & -e_3 & e_2 \\ e_3 & 0 & -e_1 \\ -e_2 & e_1 & 0 \end{bmatrix}. \tag{5}$$

Therefore, as long as the scanner measures how the object is rotated, $\boldsymbol{R}$ can be obtained. As a result, the transformation matrix $\boldsymbol{T}$ can be obtained, which is the transposed matrix of $\boldsymbol{R}$. In theory, the $\boldsymbol{T}$ can be determined by measuring the coordinate values of the positions of four points on the object before and after the rotation.

$$\begin{bmatrix} X_1 - X_0 & Y_1 - Y_0 & Z_1 - Z_0 \\ X_2 - X_0 & Y_2 - Y_0 & Z_2 - Z_0 \\ X_3 - X_0 & Y_3 - Y_0 & Z_3 - Z_0 \end{bmatrix} = \begin{bmatrix} x_1 - x_0 & y_1 - y_0 & z_1 - z_0 \\ x_2 - x_0 & y_2 - y_0 & z_2 - z_0 \\ x_3 - x_0 & y_3 - y_0 & z_3 - z_0 \end{bmatrix} \boldsymbol{T}, \tag{6}$$

where $(X_i,\ Y_i,\ Z_i)$ is the coordinate in its coordinate system with $i = 0,\ 1,\ 2,\ 3$; (x_i, y_i, z_i) is the coordinate of the same point in the platform coordinate system.

The centroid lines obtained from multiple measurements are transformed into the same coordinate system, with the results illustrated in Fig.4. By applying the least squares method, the optimal intersection coordinates can be determined, which corresponds to the centroid coordinates of the test object.

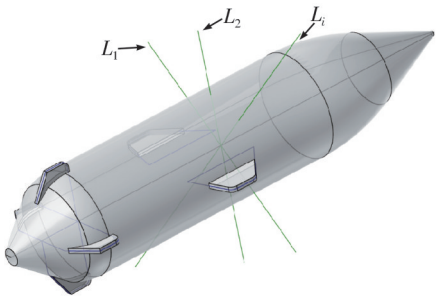

Fig. 4 Schematic diagram of centroid coordinates calculated by centroid lines

2 Results and discussion

2.1 Accuracy test of centroid measurement

To verify the accuracy of this method, a 45# steel

standard block was utilized. The standard block was first scanned and modeled as a theoretical model. And its volume was measured. By integrating the mass data and assigning appropriate density in the theoretical model, consistency between the model and the physical object was ensured. As a result, the theoretical 3D centroid could be analyzed. Then, the centroid of the standard block was measured by the prototype, which was developed by the centroid measurement method based on 3D scanning.

Fig. 5 shows the photograph of the prototype during the centroid testing. The standard block was positioned at arbitrary angles for three separate measurements. The point cloud data obtained from these measurements was then analyzed to obtain the centroid lines. The plane of the specimen stage was fitted and aligned with the XY plane of the global coordinate system to convert the whole point cloud data into the global coordinate system. The Z-axis direction corresponds to the centroid line direction. The support balls are fitted to determine their center coordinates. Combined with the weighing sensor data, the X-axis and Y-axis coordinates of the centroid line projection are calculated based on Eq. (1), thereby constructing the centroid line. The point cloud data of the test object and the centroid line are then aligned with the theoretical model.

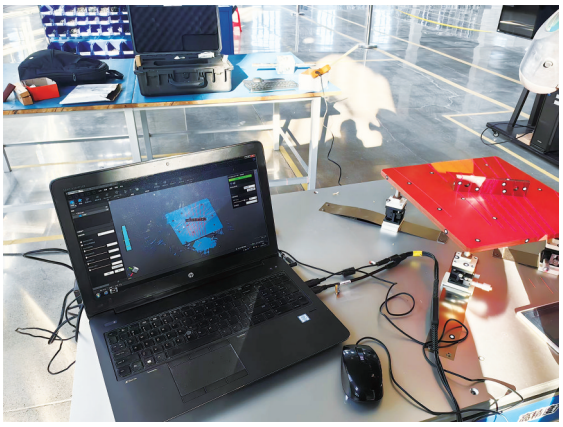

Fig. 5 Centroid measurement of standard block by prototype

Based on the data of the theoretical model and its centroid coordinate, the measurement errors can be analyzed, as detailed in Table 1. Using 3D software, the theoretical coordinates of the centroid point G for the standard component are determined to be (75.116, 4.754, 17.25). After scanning, each fitted centroid line is parameterized by two 3D coordinate points. In one experiment, the centroid lines of the standard block are defined as follows. L_1 is (111.392, 4.469, 18.953) and (−98.171, 4.469, 18.953). L_2 is (75.000, 51.471, 18.953) and (75.000, −50.572, 18.953). And L_3 is (75.000, 4.469, 66.712) and (75.000, 4.469, −48.353). Applying the least squares method to the three centroid lines, the actual measured centroid point T can be obtained. The T is (75.115, 4.749, 17.25) after three repeated experiments. As a result, the coordinate errors in the X-axis, Y-axis, and Z-axis are 0.001 mm, 0.005 mm, and 0 mm, respectively, which verifies the measurement accuracy of the prototype.

Table 1 Errors analysis of centroid measurement method based on 3D scanning

Centroid coordinate	Theoretical value/mm	Measurement value/mm	Error/mm
X	75.116	75.115	0.001
Y	4.754	4.749	0.005
Z	17.250	17.250	0
Distance		0.005	

However, in practice, parts used for industrial measurement, such as airplanes, drones, and rockets, are all complex assemblies that use a variety of materials, such as plastic, steel, aluminum, copper, and circuit boards. It is necessary to measure the centroid without disassembling the test object. Hence, a standard component with various materials and complex shapes is designed for further accuracy verification in practice, which is shown in Fig.6.

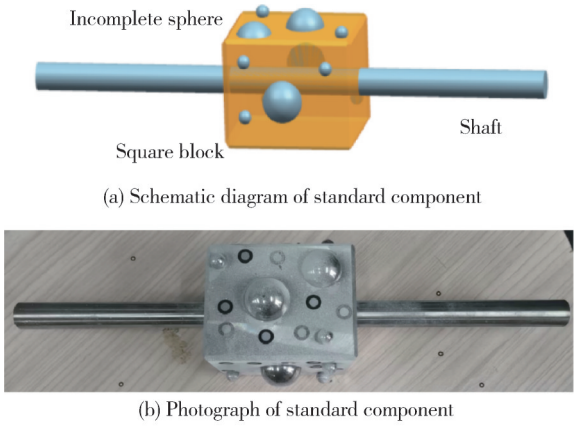

(a) Schematic diagram of standard component

(b) Photograph of standard component

Fig. 6 Standard component containing a square block, a shaft, and incomplete spheres in various sizes

It features a square block with a shaft passing through its center, onto which incomplete spheres are affixed on the other three sides. The material of the square block is aluminum, while the spheres are made of steel. Before assembly, the mass of each one was measured. The standard component was then scanned and modeled as a theoretical model. And the volumes of the individual parts were measured. By integrating the mass data and assigning appropriate densities to each material in the theoretical model, consistency between the model and the physical object was ensured. As a result, the

theoretical 3D centroid could be analyzed. Fig. 7 shows the photograph of the prototype during the centroid testing. Fig. 8 illustrates the point cloud data fitted to the theoretical model space during the first measurement state. The positions of the four support balls after fitting are indicated, with L_1 representing the position of the centroid line for this state. Similarly, the data from the three scans of the test object are converted to the coordinate system, resulting in three centroid lines being aligned within the same coordinate system, as shown in Fig. 9.

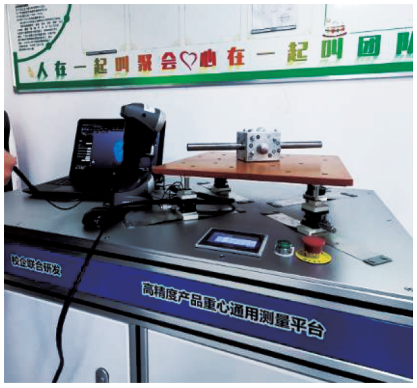

Fig. 7 Centroid measurement of standard component by prototype

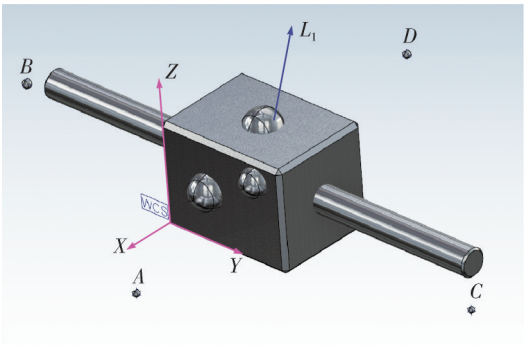

Fig. 8 Point cloud data fitted to theoretical model space

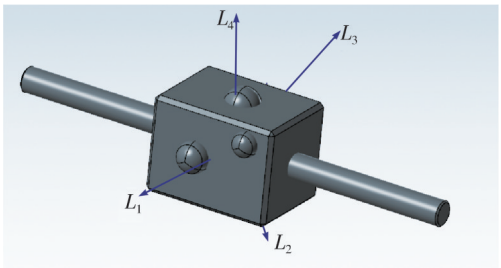

Fig. 9 Three centroid lines being aligned within the same coordinate system

The measurement error is analyzed, as detailed in Table 2. Using 3D software, the theoretical coordinates of the centroid point G for the standard component are determined to be (−40.478, 51.387, 41.121). In one experiment, the centroid lines of the standard component are defined as follows. L_1 is (165.066, 51.395, −40.480) and (−156.721, 51.395, −40.480). L_2 is (−41.013, 157.121, −40.480) and (−41.013, −178.103, −40.480). L_3 is (−41.103, 51.395, 152.072) and (−41.103, 51.395, −150.012). Applying the least squares method to the three centroid lines, the actual measured centroid point T is (−40.481, 51.396, 41.016) after three repeated experiments. As a result, the coordinate errors in the X-axis and Y-axis are 0.003 mm and 0.009 mm, respectively. The error in the Z-axis is 0.105 mm. The larger deviation in the Z-axis compared to the X-axis and Y-axis may be attributed to the interference fit between the shaft and the square block's hole during manufacturing. The shaft was driven into the hole using a striking method, causing slight deformation that resulted in theoretical discrepancies. Additionally, scanning precision and manufacturing accuracy also influence the accuracy. With increased measurement orientations and the use of accurate scanning equipment, the accuracy can be guaranteed to be within 0.1 mm.

Table 2 Errors of centroid measurement for standard component with various materials and complex shapes

Centroid coordinate	Theoretical value/mm	Measurement value/mm	Error/mm
X	−40.478	−40.481	0.003
Y	51.387	51.396	0.009
Z	41.121	41.016	0.105
Distance		0.106	

To further demonstrate the accuracy of the centroid point position, a support test was performed. The projection of the centroid onto the plane at the bottom of the square block was found. To ensure the stability of the test, the work table of the three-coordinate measuring machine is selected. The standard part is supported by a support rod with a small ball of 2 mm in diameter on the top. The results show that the standard part can be stably supported on the small plane, proving the reliability of this method, as shown in Fig. 10.

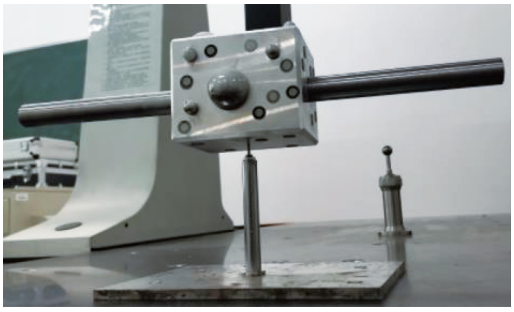

Fig. 10 Demonstration of accuracy of centroid measurement

2.2 Centroid measurement error analysis

2.2.1 Measurement error of centroid lines

Differentiating Eq. (1) can yield that

$$\mathrm{d}x=\frac{\partial x}{\partial x_A}\mathrm{d}x_A+\frac{\partial x}{\partial x_B}\mathrm{d}x_B+\frac{\partial x}{\partial x_C}\mathrm{d}x_C+\frac{\partial x}{\partial x_D}\mathrm{d}x_D+\frac{\partial x}{\partial m_A}\mathrm{d}m_A+\frac{\partial x}{\partial m_B}\mathrm{d}m_B+\frac{\partial x}{\partial m_C}\mathrm{d}m_C+\frac{\partial x}{\partial m_D}\mathrm{d}m_D, \quad (7)$$

where

$$\frac{\partial x}{\partial x_A}=\frac{m_A}{m_A+m_B+m_C+m_D},$$
$$\frac{\partial x}{\partial x_B}=\frac{m_B}{m_A+m_B+m_C+m_D},$$
$$\frac{\partial x}{\partial x_C}=\frac{m_C}{m_A+m_B+m_C+m_D},$$
$$\frac{\partial x}{\partial x_D}=\frac{m_D}{m_A+m_B+m_C+m_D},$$
$$\frac{\partial x}{\partial m_A}=\frac{(m_A+m_B+m_C+m_D)x_A}{(m_A+m_B+m_C+m_D)^2}-\frac{(x_Am_A+x_Bm_B+x_Cm_C+x_Dm_D)}{(m_A+m_B+m_C+m_D)^2}=\frac{x_A-x}{m_A+m_B+m_C+m_D},$$
$$\frac{\partial x}{\partial m_B}=\frac{x_B-x}{m_A+m_B+m_C+m_D},$$
$$\frac{\partial x}{\partial m_C}=\frac{x_C-x}{m_A+m_B+m_C+m_D},$$
$$\frac{\partial x}{\partial m_D}=\frac{x_D-x}{m_A+m_B+m_C+m_D}.$$

If there is a deviation δx_A in the X-coordinate of the support point A, it will lead to a deviation in the X-coordinate of the centroid,

$$\delta x=\frac{m_A}{m_A+m_B+m_C+m_D}\delta x_A. \quad (8)$$

Hence, if the X-coordinates of the four support points A, B, C, and D all deviate, it will result in a deviation in the X-coordinate of the centroid.

$$\begin{cases}\delta x=\dfrac{m_A}{m_A+m_B+m_C+m_D}\delta x_A+\dfrac{m_B}{m_A+m_B+m_C+m_D}\delta x_B+\dfrac{m_C}{m_A+m_B+m_C+m_D}\delta x_C+\dfrac{m_D}{m_A+m_B+m_C+m_D}\delta x_D,\\ |\delta x|\leqslant\max\limits_{i=A,B,C,D}|\delta x_i|.\end{cases} \quad (9)$$

This indicates that the error in the X-coordinate of the centroid does not exceed the upper limit of the errors in the X-coordinates of the support points. Similarly, the same conclusion holds for the Y-coordinate. This shows that the centroid coordinates are not sensitive to the coordinates of the support points. The coordinate errors of the support points are random, with both positive and negative signs, leading to a final error that is smaller than the errors in the coordinates of the support points. The scanner has a resolution of 0.05 mm and an accuracy of 0.03 mm. The accuracy can be regarded as a reference value for the expanded uncertainty. If the coverage factor $k=2$ (corresponding to a 95% confidence level), the relative uncertainty is 0.015 mm/L_m (L_m is the measured length). Considering the size of the object to be measured, the measurement error of centroid lines can be estimated as 0.01%.

2.2.2 Error of transformation matrix T

T_i is achieved by aligning the scanned point cloud data before and after the rotation of the object. In theory, T can be determined by measuring the coordinate values of the positions of four points on the object before and after the rotation, i.e.,

$$A=BT, \quad (10)$$

where $A=(X_i, Y_i, Z_i)$ is the coordinate in its coordinate system with $i=0,1,2,3$; $B=(x_i, y_i, z_i)$ is the coordinate of the same point in the platform coordinate system.

The scanning errors of the object under test before and after rotation can be expressed as δA and δB, respectively, resulting in an error of δT.

$$\begin{cases}A=B\boldsymbol{T},\\ A+\delta A=(B+\delta B)(\boldsymbol{T}+\delta\boldsymbol{T}).\end{cases} \quad (11)$$

Therefore, the relationship between the centroid l and L in different coordinate systems can be expressed as

$$L+\delta L=(l+\delta l)(\boldsymbol{T}+\delta\boldsymbol{T}). \quad (12)$$

Since the coordinates of the points on the centroid line $(L+\delta L)$ can be linearly represented by the lines of $(l+\delta l)$, the coordinate error on the centroid line does not exceed $\max(|\delta A_{i,j}|)$. And because the deviation of the point on the line only affects the position of the line when it is perpendicular to the line, the error of the line is smaller than the error of the point, that is, $|\delta L|\leqslant\max(|\delta A_{i,j}|)$.

In actual operation, a scanner is used to obtain a large amount of coordinate data, and the above equation becomes

$$\begin{bmatrix}X_1-X_0 & Y_1-Y_0 & Z_1-Z_0\\ X_2-X_0 & Y_2-Y_0 & Z_2-Z_0\\ \vdots & \vdots & \vdots\\ X_n-X_0 & Y_n-Y_0 & Z_n-Z_0\end{bmatrix}=\begin{bmatrix}x_1-x_0 & y_1-y_0 & z_1-z_0\\ x_2-x_0 & y_2-y_0 & z_2-z_0\\ \vdots & \vdots & \vdots\\ x_n-x_0 & y_n-y_0 & z_n-z_0\end{bmatrix}\boldsymbol{T}. \quad (13)$$

The T can be obtained by the least squares method. Although the data obtained by the scanner is noisy, the least squares method is equivalent to filtering the data, further suppressing the noise. There is a ready-made alignment algorithm in the scanner's supporting software, which facilitates the high-precision acquisition of T. As a result, the measurement error associated with this process can be negligible due to the high accuracy of the scanner.

2.2.3 Measurement error of mass sensors

The weighing error is determined by the precision of the mass sensor. In the calculation of centroid lines, the accuracy of the mass sensor affects the centroid's coordinates. The effect of the mass sensor A on the X-axis coordinate is shown in Eq. (7). The denominator is the square of the mass of the test object and is insensitive to coordinates. The weighing sensor has a relative error of less than $\pm 0.3\%$. Hence, the effect of mass sensor measurement error on the centroid measurement can be estimated as $\pm 0.3\%$ based on Eq. (7).

2.2.4 Evaluation of combined uncertainty

The stated combined total uncertainty was determined by taking the root sum square of the contributions of individual uncertainty sources to the total uncertainty. The expanded relative standard uncertainty is estimated to be 0.6% ($k=2$).

2.3 Centroid measurement experiments

To further investigate the reliability of this method, different types of objects were measured.

2.3.1 Verification of aircraft model centroid measurement

A model of the Airbus A380 was tested, with dimensions of 470 mm×440 mm×170 mm and a total weight of 1 410 g. The main body of the aircraft model is constructed from lightweight alloy, while the wings are made from resin. For such test objects, a dedicated testing platform and multiple custom fixtures are typically required to achieve high-precision centroid measurements. In this case, the developed prototype was utilized for the measurement. Fig. 11(a) shows the photograph of the measurement process for the aircraft model. The centroid coordinate was obtained through scanning under three different posture conditions. Before the support test, a small surface was milled out around the projection of the centroid on the bottom plane of the aircraft model. The centroid line is parallel to the normal direction of the surface. It can be seen that the airplane model can be stably supported at a certain elevation angle through the support rod, which is shown in Fig.11(b).

(a) Photograph of measurement process for aircraft model

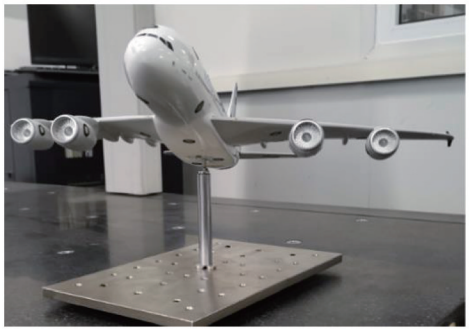

(b) Airplane model is stably supported at a certain elevation angle through a support rod

Fig. 11 Verification of aircraft model centroid measurement

2.3.2 Skull model centroid measurement

A skull model is made of cast aluminum, with dimensions of 220 mm×140 mm×130 mm and a weight of 1 894 g. It is from a critical component of a testing device. Traditional measurement methods often struggle to identify accurate and reliable reference points for positioning. However, the method based on 3D scanning technology eliminates the need for precise placement on the stage, allowing for rapid and accurate measurements. Fig.12(a) illustrates the use of the prototype for centroid measurement of the skull model. Once the centroid was determined, a supporting surface was machined. As depicted in Fig.12(b), the skull model is supported on the support rod.

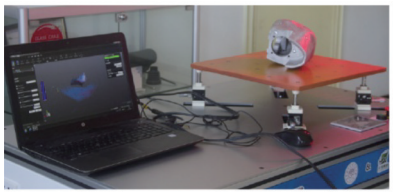

(a) Photograph of measurement process for skull model

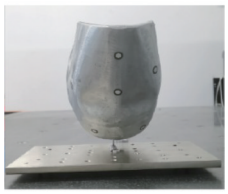

(b) Skull model is stably supported on a support rod

Fig. 12 Skull model centroid measurement

2.3.3 Pebble centroid measurement

The pebble under test has an irregular shape, and the uniformity of its material is unknown. Its dimensions are approximately 120 mm×110 mm×60 mm, with a total weight of 1 613 g. Using the prototype, centroid lines were obtained under four different posture conditions. After unifying the coordinate system, the centroid coordinates of the pebble were calculated. Finally, the pebble can be stably supported at an incline on the support rod, confirming the reliability of the centroid measurement results, which is shown in Fig.13.

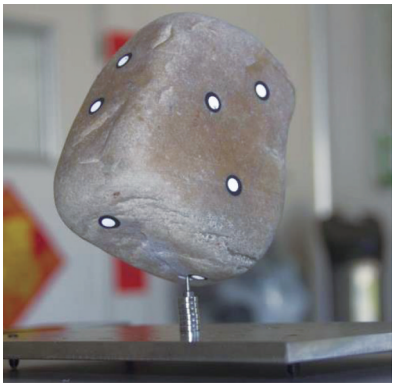

Fig. 13 Pebble with an irregular shape is stably supported at an incline on support rod

3 Conclusions

A centroid measurement method based on 3D scanning was proposed, enabling centroid measurements for different types of products on the same platform. A comparative analysis of accuracy was conducted by designing and manufacturing the standard component. Measurements of various test objects showed that the results were stable and reliable. This method eliminated the need for positioning fixtures, thereby improving measurement accuracy. Traditional methods often require the design of positioning fixtures, where positioning errors can significantly impact the measurement results. Furthermore, positioning and shape errors can compound and directly affect measurement accuracy for large components. This method provided accurate 3D data for the objects, ensuring that manufacturing and deformation errors did not influence the measurement results, thereby enhancing measurement accuracy. In the future, we will improve this method for measuring the centroid of large objects. Their centroids can be measured by dividing the large object into multiple areas, scanning them one by one, and then stitching the data of each area to generate a complete 3D model.

Acknowledgement

This work was supported by National Natural Science Foundation of China (No. 52176122).

Declaration of conflicting interests

The authors have no conflict of interests related to this publication.

References

[1] ZHANG X L, YU H, TANG W Y, et al. General mass property measurement equipment for large-sized aircraft. Sensors, 2022, 22(10): 3912.

[2] YANG Y, ZHAO M R, LI D T, et al. A disturbance suppression micro-Newton force sensor based on shadow method. ISA Transactions, 2023, 134: 442-450.

[3] YANG Y, ZHAO M R, HUANG Y G, et al. Micro-force sensing techniques and traceable reference forces: a review. Measurement Science and Technology, 2022, 33(11): 114010.

[4] LI S G, CHU W M, HUANG X. Measurement method of aircraft barycenter based on multi posture. Sensor Review, 2020, 40(2): 217-226.

[5] SUN B, ZHENG G, ZHANG X X. Application of contact laser interferometry in precise displacement measurement. Measurement, 2021, 174: 108959.

[6] LI W Y, HU J H, SU Z Z, et al. Analysis and design of axial inductive displacement sensor. Measurement, 2022, 187: 110159.

[7] MODENINI D, CURZI G, TORTORA P. Experimental verification of a simple method for accurate center of gravity determination of small satellite platforms. International Journal of Aerospace Engineering, 2018, 2018(1): 3582508.

[8] PREVIATI G, GOBBI M, MASTINU G. Measurement of the mass properties of rigid bodies by means of multi-filar pendulums-Influence of test rig flexibility. Mechanical Systems and Signal Processing, 2019, 121: 31-43.

[9] YU H, ZHANG X L, WANG Z Q, et al. Research on the pose error compensation technology for the mass and centroid measurement of large-sized aircraft based on kinematics. Sensors, 2023, 23(2): 701.

[10] LI T, SHANGGUAN W B, YIN Z H. Error analysis of inertia parameters measurement for irregular-shaped rigid bodies using suspended trifilar pendulum. Measurement, 2021, 174: 108956.

[11] MONDAL N, ACHARYYA S, SAHA R, et al. Optimum design of mounting components of a mass property measurement system. Measurement, 2016, 78: 309-321.

[12] ZHANG M W, LIU D T, LIU Y M. Recent progress in precision measurement and assembly optimization methods of the aero-engine multistage rotor: a comprehensive review. Measurement, 2024, 235: 114990.

[13] BACARO M, CIANETTI F, ALVINO A. Device for measuring the inertia properties of space payloads. Mechanism and Machine Theory, 2014, 74: 134-153.

[14] YANG Y, ZHAO M R, HUANG Y G, et al. Development of a nanoscale displacement sensor based on the shadow method. Applied Optics, 2022, 61(22): G9-G14.

[15] CHEN L, ZHANG D W, ZHOU Y L, et al. Design of a high-precision and non-contact dynamic angular displacement measurement with dual-Laser Doppler Vibrometers. Scientific Reports, 2018, 8(1): 9094.

[16] LI R R, LIU Y M, TAN J B. Determination of COG based on propagation of positioning and orientation errors in aero-engine rotors. IEEE Transactions on Instrumentation

and Measurement, 2022, 71: 1004611.
[17] WANG M B, ZHAO S. Research on error separation method of center of gravity measurement system for large-sized solid of revolution. Measurement Science and Technology, 2023, 34(9): 095019.
[18] WANG M B, ZHANG X L, TANG W Y, et al. A structure for accurately determining the mass and center of gravity of rigid bodies. Applied Sciences, 2019, 9(12): 2532.
[19] GONZALO O, SEARA J M, CHEKH B A, et al. A method for the 3D identification of the center of gravity of an aircraft. Measurement, 2023, 220: 113398.
[20] OMIDALIZARANDI M, PAFFENHOLZ J A, NEUMANN I. Automatic and accurate passive target centroid detection for applications in engineering geodesy. Survey Review, 2019, 51(367): 318-333.

基于三维扫描的质心测量方法

何 欣[1], 黎 振[2*]

1. 天津职业技术师范大学 工程实训中心, 天津 300222;
2. 天津职业技术师范大学 机械工程学院, 天津 300222

摘 要: 质心坐标是飞机、导弹、火箭、无人机等运动系统的关键控制参数, 直接影响其运动动力学和控制性能。传统的质心测量方法往往需要定制设备和专门的定位装置, 成本高, 精度有限。本文提出了一种集成三维(3D)扫描技术的新型质心测量技术, 无需专用的定位装置, 即可精确测定各种物体类型的质心参数, 提高了质心测量系统的通用性和精度。我们建立了一个将称重法原理与3D扫描技术相结合的质心测量理论框架, 使用标准组件严格评估了该技术的测量精度, 揭示了多个坐标方向上的精确精度指标。通过对三种不同类型的产品进行实验验证, 进行了定性验证。实验结果表明, 以设计的标准件为检测对象, X、Y、Z方向的质心理论值与实测值偏差分别为0.003 mm, 0.009 mm, 0.105 mm, 三维空间偏差为0.106 mm。验证了该方法的可靠性, 可实现各类产品质心的高精度测量, 无需定位工装。该成果大大拓展了质心测量装置的适用性和测量范围, 为复杂零件及系统的精密测量提供了新的理论依据和方法。

关键词: 质心测量; 质量参数; 三维扫描; 三维点云数据; 无定位装置; 多点称重法

引用格式: HE Xin, LI Zhen. A centroid measurement method based on 3D scanning. Journal of Measurement Science and Instrumentation, 2025, 16(2): 186-194. DOI: 10.62756/jmsi.1674-8042.2025018